sensors

MDPI

Article

InGaN as a substrate for AC photoelectrochemical imaging

Bo Zhou [1], Anirban Das [1], Menno J. Kappers [2], Rachel A. Oliver [2], Colin J. Humphreys [1], Steffi Krause [1,*]

[1] School of Engineering and Materials Science, Queen Mary University of London, Mile End Road, London E1 4NS, UK

[2] Department of Materials Science and Metallurgy, University of Cambridge, 27 Charles Babbage Road, Cambridge CB3 0FS, UK

* Correspondence: s.krause@qmul.ac.uk.

Received: date; Accepted: date; Published: date

Abstract: AC photoelectrochemical imaging at electrolyte-semiconductor interfaces provides spatially resolved information such as surface potentials, ion concentrations and electrical impedance. In this work, thin films of InGaN/GaN were used successfully for AC photoelectrochemical imaging, and experimentally shown to generate a considerable photocurrent under illumination with a 405 nm modulated diode laser at comparatively high frequencies and low applied DC potentials, making this a promising substrate for bioimaging applications. Linear sweep voltammetry showed negligible dark currents. The imaging capabilities of the sensor substrate were demonstrated with a model system and showed a lateral resolution of 7 microns.

Keywords: Photoelectrochemistry; InGaN/GaN epilayer; cell imaging; light-activated electrochemistry; light-addressable potentiometric sensor.

1. Introduction

Over the past three decades since first proposed by Hafeman et al. in 1988 [1], photocurrent imaging with light-addressable potentiometric sensors (LAPS) has received increasing attention for chemical and biological applications such as the detection of ions [2], redox potentials [3], enzymatic reactions [4] and cellular activities [5][6][7]. By scanning a designated area of an electrolyte–insulator–semiconductor (EIS) structure with a modulated light beam, spatiotemporal AC photocurrent images with the two-dimensional distribution of analytes are produced [8][9].

To enhance the spatial resolution and photocurrent response, a wide range of semiconductor substrates have been investigated. Silicon on insulator (SOI) [10][11], ultrathin silicon on sapphire (SOS) [12] and semiconductor materials such as amorphous silicon, GaAs [13], GaN [14], TiO_2 [15] and In-Ga-Zn oxide [16] were studied. SOS substrates exhibited a high resolution of 1.5 μm with a focused 405 nm laser beam and a resolution of 0.8 μm using a two-photon effect with a 1250 nm femtosecond laser [12]. SOS functionalized with self-assembled monolayers (SAMs) as an insulator has been used for imaging of chemical patterns [17][18][19], microcapsules [20]and yeast cells [21]. Modifying silicon with SAMs terminated with redox active species allowed the imaging of photo-induced redox currents [22].

Recently, ITO-coated glass without any insulator was proposed as a low cost and robust substrate for photoelectrochemical imaging [23][24]. In the absence of an insulator, the AC photocurrent is largely determined by the anodic oxidation of hydroxide making ITO-LAPS highly sensitive to pH (70 mV/pH). Photocurrent imaging with ITO-LAPS showed a good lateral resolution of 2.3 μm [23] and was confirmed to be sensitive to the surface charge of living cells [24]. ZnO nanorods were used as a substrate for ac photocurrent imaging to monitor the degradation of

a thin poly (ester amide) film with the enzyme α-chymotrypsin, also showing great potential in biosensing and bioimaging applications [25]. However, a relatively high applied bias (1.5 V) was required to achieve sufficiently high photocurrents with ITO and ZnO nanorods for two-dimensional imaging, which could possibly interfere with cellular metabolism. Moreover, due to low charge carrier mobility, both ITO and ZnO suffered a dramatic decrease in photocurrent with increasing modulation frequency, resulting in a low working frequency of 10 Hz for imaging. This could consequently limit their application for high-speed imaging which is required for the investigation of cellular responses.

In this work, InGaN/GaN on sapphire was investigated as a new substrate for AC photoelectrochemical imaging, aiming to solve the above-mentioned problems. InGaN is a semiconductor alloy with a direct band gap that can be tuned from the near-infrared (0.6 eV, InN) to the ultraviolet (3.4 eV, GaN) by adjusting the indium concentration. It has been used widely in developing LEDs [26][27] and photovoltaic devices [28] owing to its strong light emission and absorption and a wide range of band gaps. InGaN has also gained significant attention in photoelectrochemistry. With band edges straddling oxygen and hydrogen redox overpotentials, p-type GaN/InGaN nanowires have been investigated in water splitting [29] with advantages of high carrier mobility, good chemical stability, and band gap tunability. GaN/InGaN nanowires have also been shown to exhibit excellent optochemical and electrochemical sensor performance, achieving the detection of pH [30], oxidising gases (O_2, NO_2 and O_3) [31] through photoluminescence, and electrochemical detection of nicotinamide adenine dinucleotide (NADH) [32]. In this work, it will be shown that epitaxial layers of InGaN are suitable for photoelectrochemical imaging with good lateral resolution and have great potential in bioimaging applications.

2. Experimental section

Materials.

The InGaN/GaN structure was grown on a two-side polished (0001) sapphire substrate in a Thomas Swan 6x2" metalorganic vapour-phase epitaxy reactor using trimethyl gallium (TMG), trimethyl indium (TMI), silane (SiH_4) and ammonia (NH_3) as precursors, while purified hydrogen and nitrogen were used as the carrier gases. A 40 nm-thick low-temperature (580 °C) GaN nucleation layer was followed by a 100 nm-thick n-type GaN layer deposited at 1060 ºC in a hydrogen atmosphere at a constant pressure of 100 Torr. The carrier gas was then switched to nitrogen, the pressure ramped at 300 Torr and the temperature to 770 ºC for the growth of the 100 nm-thick n-type InGaN epilayer.

All wet chemicals were purchased from Sigma-Aldrich. All solutions in this work were prepared using ultrapure water (18.2 MΩ cm) from a Milli-Q water purification system (Millipore, USA).

Preparation and characterisation of sensor chip.

The InGaN/GaN structure was cut into 5 mm × 5 mm pieces. These were ultrasonically cleaned with acetone, isopropanol and ultrapure water each for 15 min and blow dried with nitrogen. The InGaN/GaN samples were kept at room temperature before use. The morphology of InGaN/GaN was examined using a scanning electron microscope (SEM, FEI Inspect F). Ultraviolet–visible (UV-vis) spectra were obtained using a UV−vis spectrometer (PerkinElmer, Lamda 950).

Linear sweep voltammetry (LSV).

LSV of InGaN/GaN was carried out in Dulbecco's Phosphate Buffered Saline (DPBS) solution (pH 7.4) using an Autolab PGSTAT30/FRA2 electrochemical workstation (Windsor Scientific Ltd., UK). A platinum electrode and an Ag/AgCl (3 M KCl) electrode were the counter electrode and reference electrode, respectively. The scan rate was 10 mV/s. A diode laser (λ = 405 nm, max 50 mW), chopped in 10 s intervals was used as the light source while recording the LSV curves.

Cell culture.

Before seeding cells, InGaN substrates were sterilized with 70% ethanol and rinsed thoroughly with sterilized DPBS solution and blown dry. MG-63 human osteosarcoma cells were cultivated in Dulbecco's Modified Eagle's Medium (DMEM, Cat No D6429) supplemented with 10% Fetal Bovine Serum (FBS, Cat No F9665 and 1% penicillin-streptomycin (Cat No P4333)in an air jacketed incubator with 5% CO_2 at 37 °C with the medium changed every two days. At 70%-80% confluence, cells were trypsinized by using Trypsin-EDTA (Cat No T3924), and resuspended in 10 % FBS supplemented DMEM, seeded onto the InGaN surface at a concentration of $2.5x10^4$ cells/mL and incubated at 37 °C with 5% CO_2 for 24 h.

The cell viability was tested using a fluorescence live/dead assay (Thermo Fisher Scientific, cat. no.: L3224). MG-63 cells were seeded onto two pieces of InGaN (5 mm × 5 mm) assembled in the photoelectrochemical imaging chamber at a concentration of $9.4x10^5$ cells/mL and incubated at 37 °C with 5% CO_2 for 24 h. One InGaN chip was subjected to a raster scan in DPBS while another stayed under ambient condition for the same time. Then, 0.5 mL of 2 μM calcein AM, 4 μM Ethidium homodimer-1 and 8.12 μM of Hoechst 33342 was used to detect the viability of the cells with and without AC photoelectrochemical imaging. Three different areas in each sample were checked using a fluorescence microscope (Leica DMI4000B Epifluorescence), and cell photos were then processed by Image J software for counting cells.

AC photocurrent imaging.

Figure 1 depicts the LAPS set-up used in this work. A diode laser LD1539 (Laser 2000, λ = 405 nm, max 50 mW) intensity modulated at 1 kHz was used as the light source. The sample chamber was mounted onto an M-VP-25XL XYZ positioning system with a 50 nm motion sensitivity on all axes (Newport, UK). AC photocurrents were measured with an EG&G 7260 lock-in amplifier with a platinum electrode and an Ag/AgCl (3 M KCl) electrode acting as the counter and reference electrodes, respectively. DPBS (pH 7.4) was used as the electrolyte. Optical images of the sensor surface were obtained with a CMOS camera by illuminating the chip surface with white light from the front side. A drop of poly(methyl methacrylate) (PMMA) was deposited on the InGaN surface and dried overnight to obtain a model system for measuring the resolution.

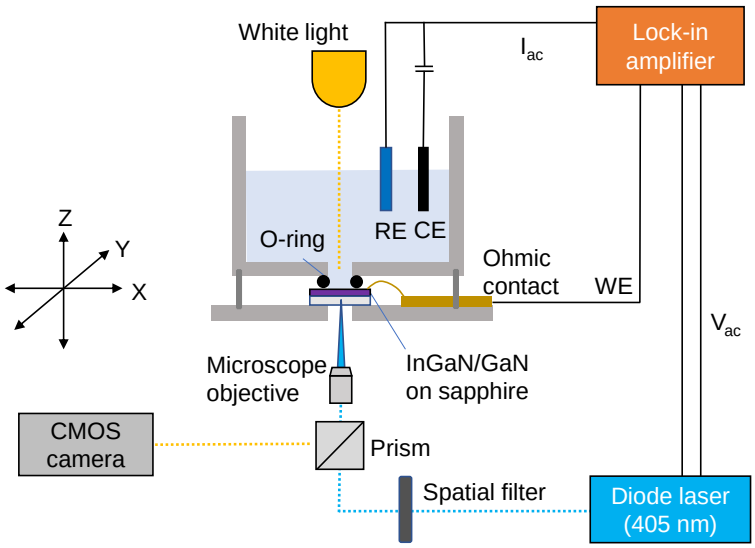

Figure 1. Schematic of the LAPS setup with a 405 nm diode laser to generate photo-induced charge carriers, lock-in amplifier to measure AC photocurrent, and an X-Y-Z stage to move the electrochemical cell with respect to the laser beam for imaging.

3. Results and discussion

Characterisation of InGaN/GaN epilayers on sapphire.

The SEM analysis of the InGaN/GaN structure is presented in Figure 2. The SEM top view in Figure 2a shows the InGaN surface with a high density of pits ((2.26 ± 0.08) x 10^{10} pits/cm^2) ranging between 20 nm and 50 nm in diameter, as some of the pits have merged. These "V-pits" are well known in InGaN growth and consist of an inverted hexagonal pyramid emanating from a threading dislocation formed at the sapphire/GaN interface. The pits open up during InGaN growth which takes place at relatively low temperatures [33]. The total thickness of the InGaN/GaN epilayer was about 216.5 ± 6.6 nm as shown in Figure 2b. Four-probe electrical measurements using soldered indium contacts showed a resistivity of 0.02 Ω·cm due to the n-type conductivity of the epilayers. A photoluminescence (PL) spectral map (Accent RPM2000, exc = 266 nm) of the 2-inch wafer showed a strong emission band centred at 448 ± 2 nm indicating an average indium fraction of ca. 17.5% [34].

Figure 3 shows the UV-vis absorption spectrum of InGaN/GaN. From the inset Tauc-plot [35], [36], a direct band gap of 2.77 ± 0.03 eV was determined, indicating that the charge carriers in InGaN/GaN are excited at wavelengths ≤ 448 nm, which is in good correspondence with the PL mapping result.

The DC photocurrent response of the InGaN/GaN sample was characterised with LSV. As shown in Figure 4, significant photocurrents were observed at anodic potentials ≥ 0 V. The dark current was negligible compared to the photocurrent. As with ITO substrates, the photocurrent can be ascribed to the oxidation of hydroxide ions in the solution. In contrast to ITO, the InGaN layers show a much lower onset potential of the photocurrent.

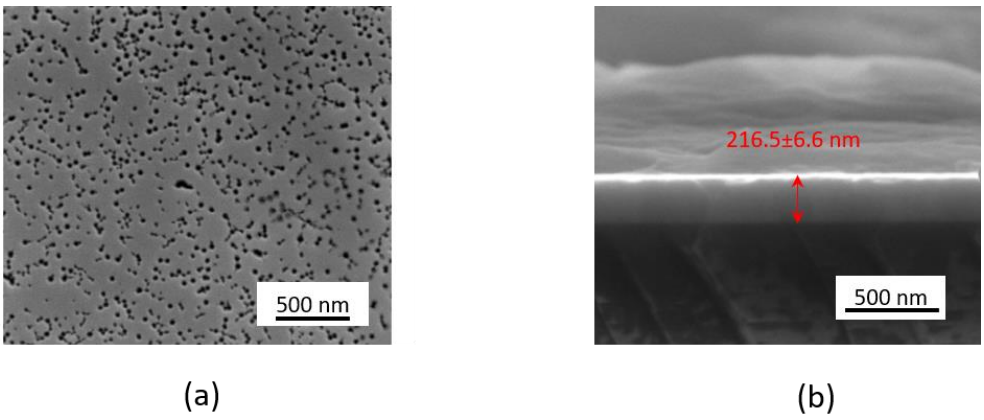

Figure 2. SEM images of InGaN/GaN: (a) top view and (b) cross-sectional view.

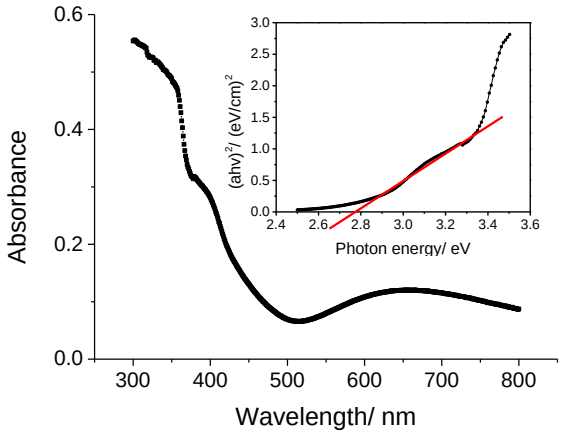

Figure 3. UV−vis spectrum of InGaN and inset Tauc-plot.

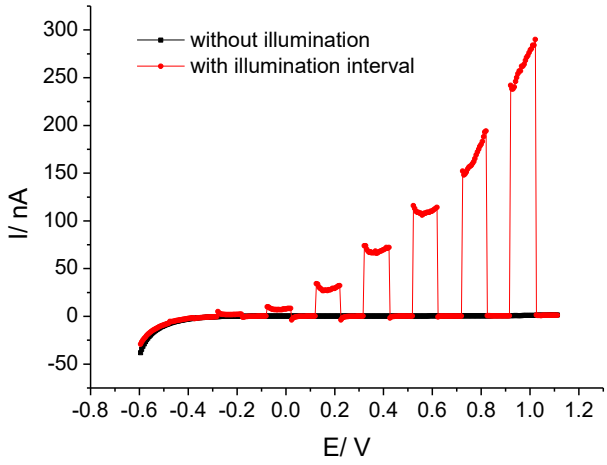

153

154 **Figure 4.** LSV curves of InGaN in the dark and with chopped illumination.

155 Figure 5a shows the dependence of the AC photocurrent on the modulation frequency
156 measured at 1.0 V with a focused laser beam. From 10 Hz to 3 kHz, the photocurrent did not change
157 significantly with the frequency and then it decreased at higher frequencies. Significant
158 photocurrents were obtained up to modulation frequencies of 10 kHz. The photocurrent became
159 negligible at frequencies greater that 20 kHz. In contrast, the AC photocurrent measured with ITO
160 and ZnO previously decreased continuously with increasing modulation frequency above 10 Hz for
161 ITO and above 30 Hz for ZnO and became negligible at 7 kHz for ITO and 4 kHz for ZnO. This can
162 be attributed to the significantly higher hole mobilities in InGaN [37] compared to those in ITO [38]
163 and ZnO [39] as low-mobility minority charge carriers will not contribute to the AC photocurrent at
164 high frequencies. In this work, 1 kHz was chosen as the modulation frequency since it could offer
165 high quality images as well as demonstrate the potential for high-speed imaging.
166

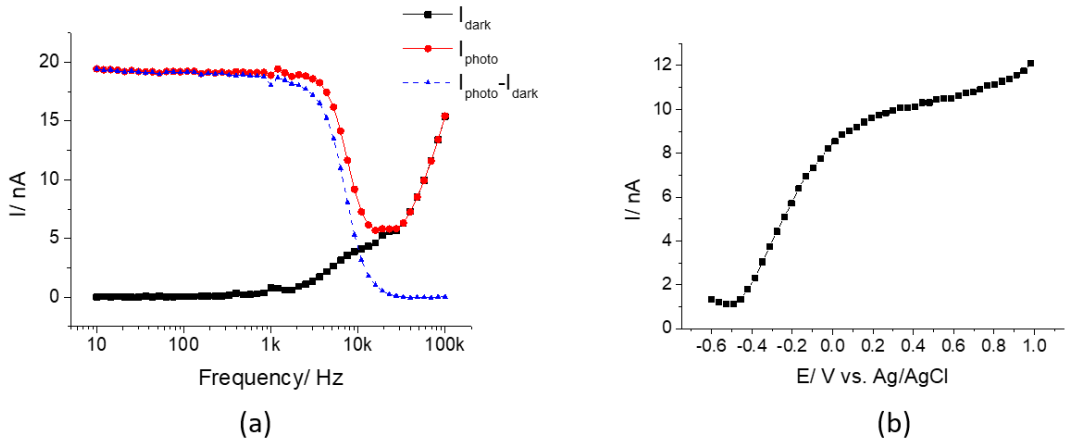

167

168 **Figure 5.** (a) Frequency dependence of the AC photocurrent and the background dark current
169 measured at 1.0 V; (b) Characteristic I–V curve of InGaN/GaN measured in pH 7.4 DPBS at 1 kHz
170 with a focused laser beam at 18% maximum intensity.

171 Figure 5b shows the characteristic AC photocurrent–voltage (*I*–*V*) curve of InGaN/GaN in the
172 voltage range -0.6 V to 1.0 V in pH 7.4 DPBS under the illumination of a focused laser beam
173 (modulation frequency was 1 kHz). It shows that the photocurrent increased with the applied bias,
174 to a value of 12 nA at 1.0 V. Even at 0 V, a photocurrent of 8.5 nA was observed. The low onset
175 potential of InGaN/GaN is in accordance with its low flat band potential [40][41], indicating that the
176 electrode can become depleted by applying a low bias, facilitating the separation of photo-induced
177 charge carriers. Therefore, it provides the possibility for measurements at zero applied bias.

Photoelectrochemical imaging using InGaN

Figures 6a and 6b shows the photocurrent images of a PMMA dot on the InGaN surface with a modulation frequency of 1 kHz using a focused laser beam at a bias of 0.6 V and 0 V (vs. Ag/AgCl) respectively. The polymer dots were clearly observed in the photocurrent images, with decreased photocurrent values compared to a blank surface area owing to the high impedance of the PMMA dot. The image in Figure 6a shows a significant gradient of the photocurrent across the uncoated area exposed to electrolyte. This can be attributed to the sample not being mounted perfectly perpendicular to the incoming laser beam resulting in a change of the focused laser spot size across the sample. Where applications require imaging over a large area, a tilt module for straightening the sample would have to be integrated into the experimental setup. However, for imaging over small distances, this effect becomes negligible as will become clear in the next section. The images in Figure 6b and less obviously in Figure 6a display a periodic pattern in the photocurrent distribution. It is assumed that this is caused by a striation effect in the InGaN/GaN substrate similar to the one observed in silicon previously [42] It is worth noting that the ability to image at 0 V will broaden the application of this technique in biological systems and also possesses an advantage from an energy aspect. To measure the lateral resolution, a photocurrent line scan across the edge of the polymer film was recorded with a focused laser beam and 1 µm step size (Figure 6c). The lateral resolution is derived from the full width at half maximum (FWHM) value of the first derivative of the line [43] (Figure 6d), which is 7 µm for InGaN. This result could be due to a weak adhesion between PMMA and the InGaN surface, thus not giving a steep edge of the polymer, or light scattering within the structure. The diffusion length of minority charge carriers in InGaN should not affect the resolution as it is less than 200 nm and decreases with increasing In content [44]. Hence, InGaN is promising to produce photocurrent images with a higher resolution.

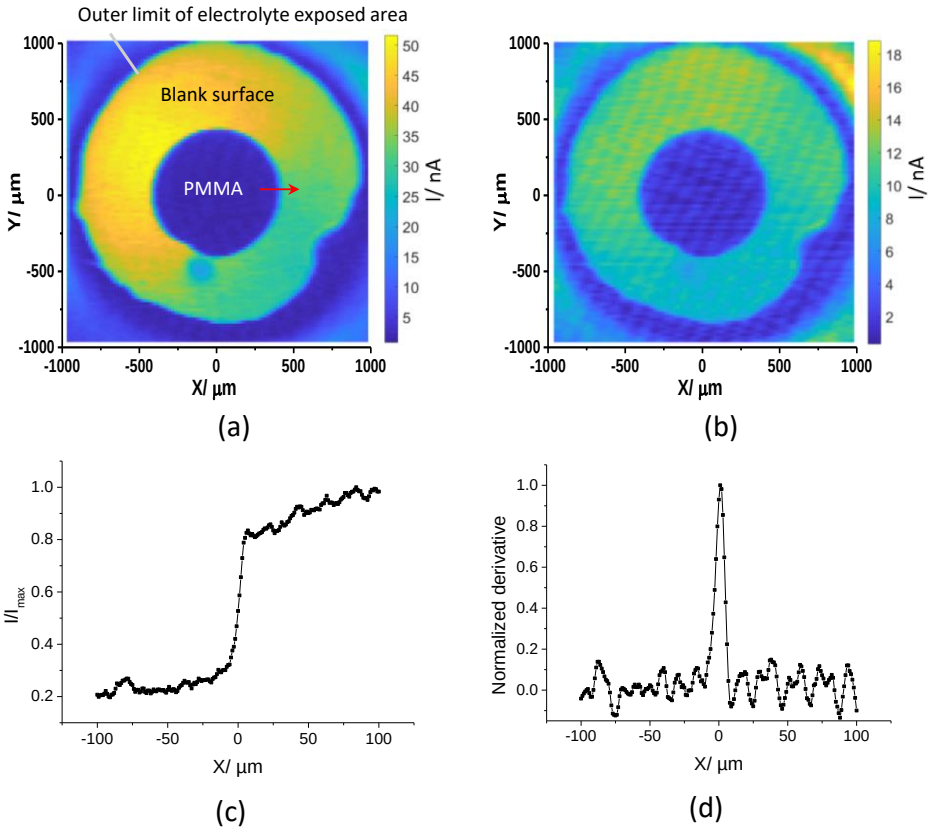

Figure 6. AC photocurrent images of a PMMA dot on InGaN measured at 0.6 V (a) and 0 V (b); X axis line scan across the polymer edge (indicated by the red arrow in (a)) at 0.6 V (c) and its corresponding first derivative plot (d).

Cell imaging on InGaN

Figure 7a shows a photocurrent image of an MG-63 cell seeded on the InGaN surface obtained at a bias of 1.05 V, with a light modulation frequency of 1 kHz. The cell profile is clearly observed, as the photocurrent is smaller in the cell attachment area than on the blank surface. Both, photocurrent image and the corresponding optical image (Figure 7b) show good correlation. Apart from the cell in the centre of the image (outline superimposed in blue in Figure 7a), another three cells are visible towards the edges (outlines superimposed in red in Figure 7a). As the latter cells are rounded, it can be assumed that they are not attached to the sensor surface and do therefore not cause a significant change in the local photocurrent. The photocurrent under a cell attached to the semiconductor surface is affected by the narrow gap (> 10 nm) formed between the cell membrane and the surface as described previously for cells cultured on ITO [24]. The photocurrent is caused by the oxidation of hydroxide. Transport of hydroxide to the surface is hindered by diffusion into the narrow electrolyte gap between cell and surface, thereby reducing the photocurrent under the cell. The negative surface charge of the cell causes an additional reduction in the transport of hydroxide ions to the surface. Hence, a correlation between the photocurrent and the cell surface charge was found [24].

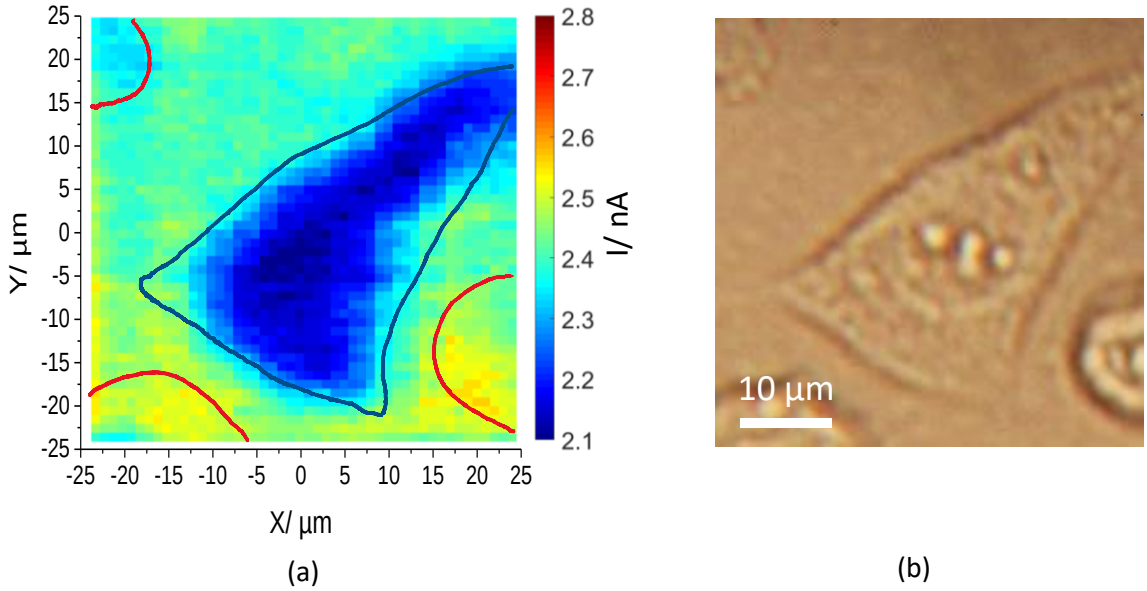

Figure 7. (a) AC photocurrent image of a mesenchymal stem cell on InGaN surface (cell shapes from (b) superimposed in blue for an attached cell and red for non-attached cells) and (b) its corresponding optical image.

Cell viability.

To check the invasiveness of InGaN-based AC photocurrent imaging, cell viability for cells with and without AC photocurrent raster scan were tested (Figure 8). Calcein AM can permeate through intact cell membranes and react with the intracellular enzyme esterase, giving an intensely green fluorescence in live cells (excitation/emission 495 nm/515 nm). Ethidium homodimer-1 only passes through disrupted membranes, emitting intense red fluorescence in dead cells upon binding to nucleic acids (excitation/emission 495 nm/635 nm). Hoechst stain is a cell-permeant nuclear counterstain that emits blue fluorescence when bound to dsDNA (excitation/emission 350 nm/461 nm) to determine cell numbers. Results shows that 98.92% ± 0.15% MG-63 cells on the surface were viable after a photocurrent raster scan compared to 98.97% ± 0.11% on a control sample, indicating this imaging technique has no negative effect on the cells.

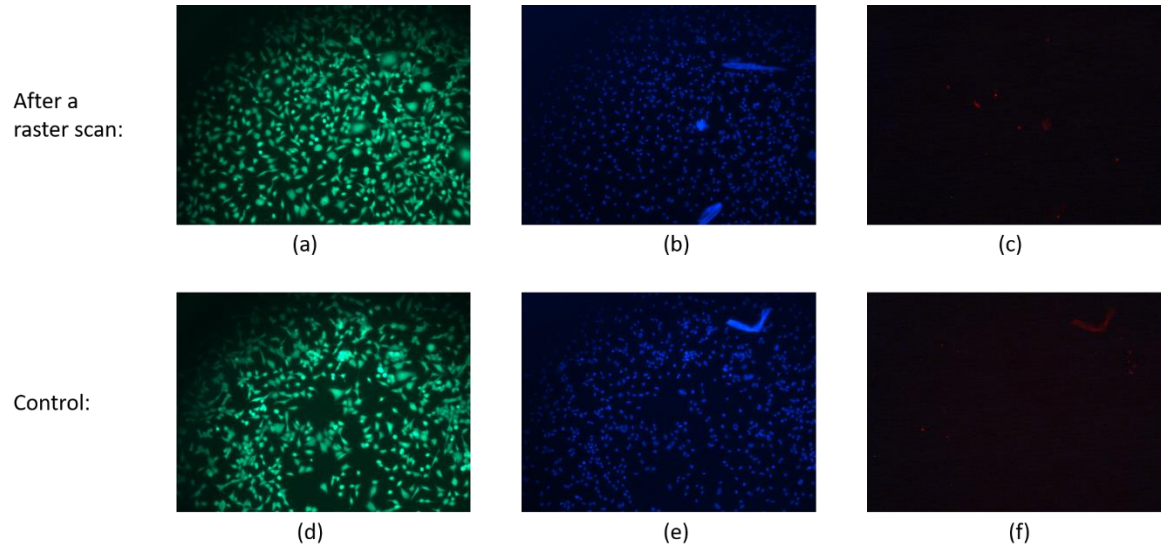

Figure 8. (a)(b)(c) Fluorescence microscope images of MG-63 cells taken after photocurrent imaging, living cells with intact membranes appeared green, dead cells with collapsed membrane appeared red, and the nuclei of the cells appeared blue. (d)(e)(f) Images of MG-63 cells that were not subjected to imaging.

4. Conclusions

An $In_{0.175}Ga_{0.825}N$/GaN structure on sapphire was investigated as a substrate for photocurrent imaging without any modification. It showed a considerable photocurrent under illumination with a 405 nm diode laser. Clear photocurrent images of a PMMA dot were obtained with a focused laser beam at 1 kHz modulation frequency, indicating a unique advantage over ITO and ZnO studied previously. In addition, photocurrent imaging at a low bias (0 V) was demonstrated and photocurrent imaging of a cell was achieved, showing a great potential of InGaN for applications in bioimaging and biosensing.

Acknowledgements

The authors are grateful to the China Scholarship Council for providing a PhD studentship to B. Zhou, to the EU for providing a Marie Skłodowska-Curie Individual Fellowship to A. Das (H2020-MSCA-IF-2016-745820) and to EPSRC (EP/R035571/1) for funding.

Author contributions

B.Z. carried out the measurements and prepared the original draft. A.D. contributed to the data analysis and edited the paper. M.J.K. fabricated the InGaN/GaN, carried out photoluminescence and resistance measurements and co-wrote the paper. R.A.O., C.J.H and S.K. contributed to the experimental design and the interpretation of data and co-wrote the paper

References

1. Hafeman, D.G.; Parce, J.W.; McConnell, H.M. Light-addressable potentiometric sensor for biochemical systems. *Science (80-.).* **1988**, *240*, 1182 LP – 1185.
2. Mourzina, Y.; Yoshinobu, T.; Schubert, J.; Lüth, H.; Iwasaki, H.; Schöning, M.J. Ion-selective light-addressable potentiometric sensor (LAPS) with chalcogenide thin film prepared by pulsed laser deposition. *Sensors Actuators, B Chem.* **2001**, *80*, 136–140.
3. Oba, N.; Yoshinobu, T.; Iwasaki, H. Redox Potential Imaging Sensor. *Jpn. J. Appl. Phys.* **1996**, *35*, L460–

L463.
4. Seki, A.; Ikeda, S.; Kubo, I.; Karube, I. Biosensors based on light-addressable potentiometric sensors for urea, penicillin and glucose. *Anal. Chim. Acta* **1998**, *373*, 9–13.
5. Poghossian, A.; Ingebrandt, S.; Offenhäusser, A.; Schöning, M.J. Field-effect devices for detecting cellular signals. *Semin. Cell Dev. Biol.* **2009**, *20*, 41–48.
6. Hu, N.; Wu, C.; Ha, D.; Wang, T.; Liu, Q.; Wang, P. A novel microphysiometer based on high sensitivity LAPS and microfluidic system for cellular metabolism study and rapid drug screening. *Biosens. Bioelectron.* **2013**, *40*, 167–173.
7. Dantism, S.; Takenaga, S.; Wagner, T.; Wagner, P.; Schöning, M.J. Differential imaging of the metabolism of bacteria and eukaryotic cells based on light-addressable potentiometric sensors. *Electrochim. Acta* **2017**, *246*, 234–241.
8. Owicki, J.C.; Bousse, L.J.; Hafeman, D.G.; Kirk, G.L.; Olson, J.D.; Wada, H.G.; Parce, J.W. The Light-Addressable Potentiometric Sensor: Principles and Biological Applications. *Annu. Rev. Biophys. Biomol. Struct.* **1994**, *23*, 87–114.
9. Wu, F.; Campos, I.; Zhang, D.W.; Krause, S. Biological imaging using light-addressable potentiometric sensors and scanning photo-induced impedance microscopy. *Proc. R. Soc. A Math. Phys. Eng. Sci.* **2017**, *473*.
10. Ito, Y. High-spatial resolution LAPS. *Sensors and Actuators B-Chemical* **1998**, *52*, 107–111.
11. Krause, S.; Talabani, H.; Xu, M.; Moritz, W.; Griffiths, J. Scanning photo-induced impedance microscopy - An impedance based imaging technique. *Electrochim. Acta* **2002**, *47*, 2143–2148.
12. Chen, L.; Zhou, Y.; Jiang, S.; Kunze, J.; Schmuki, P.; Krause, S. High resolution LAPS and SPIM. *Electrochem. commun.* **2010**, *12*, 758–760.
13. Moritz, W.; Gerhardt, I.; Roden, D.; Xu, M.; Krause, S. Photocurrent measurements for laterally resolved interface characterization. *Fresenius. J. Anal. Chem.* **2000**, *367*, 329–333.
14. Das, A.; Chang, L.B.; Lai, C.S.; Lin, R.M.; Chu, F.C.; Lin, Y.H.; Chow, L.; Jeng, M.J. GaN Thin Film Based Light Addressable Potentiometric Sensor for pH Sensing Application. *Appl. Phys. Express* **2013**, *6*.
15. Suzurikawa, J.; Nakao, M.; Jimbo, Y.; Kanzaki, R.; Takahashi, H. A light addressable electrode with a TiO_2 nanocrystalline film for localized electrical stimulation of cultured neurons. *Sensors Actuators, B Chem.* **2014**, *192*, 393–398.
16. Yang, C.; Chen, C.; Chang, L.; Lai, C. IGZO Thin-Film Light-Addressable Potentiometric Sensor. *IEEE Electron Device Lett.* **2016**, *37*, 1481–1484.
17. Wang, J.; Wu, F.; Watkinson, M.; Zhu, J.; Krause, S. "click" Patterning of Self-Assembled Monolayers on Hydrogen-Terminated Silicon Surfaces and Their Characterization Using Light-Addressable Potentiometric Sensors. *Langmuir* **2015**, *31*, 9646–9654.
18. Wang, J.; Zhou, Y.; Watkinson, M.; Gautrot, J.; Krause, S. High-sensitivity light-addressable potentiometric sensors using silicon on sapphire functionalized with self-assembled organic monolayers. *Sensors Actuators B Chem.* **2015**, *209*, 230–236.
19. Wu, F.; Zhang, D.W.; Wang, J.; Watkinson, M.; Krause, S. Copper Contamination of Self-Assembled Organic Monolayer Modified Silicon Surfaces Following a "Click" Reaction Characterized with LAPS and SPIM. *Langmuir* **2017**, *33*, 3170–3177.
20. Wang, J.; Campos, I.; Wu, F.; Zhu, J.; Sukhorukov, G.B.; Palma, M.; Watkinson, M.; Krause, S. The effect of gold nanoparticles on the impedance of microcapsules visualized by scanning photo-induced impedance microscopy. *Electrochim. Acta* **2016**, *208*, 39–46.
21. Zhang, D.W.; Wu, F.; Wang, J.; Watkinson, M.; Krause, S. Image detection of yeast Saccharomyces cerevisiae by light-addressable potentiometric sensors (LAPS). *Electrochem. commun.* **2016**, *72*, 41–45.
22. Vogel, Y.B.; Gooding, J.J.; Ciampi, S. Light-addressable electrochemistry at semiconductor electrodes: redox imaging, mask-free lithography and spatially resolved chemical and biological sensing. *Chem. Soc. Rev.* **2019**, 3723–3739.
23. Zhang, D.W.; Wu, F.; Krause, S. LAPS and SPIM Imaging Using ITO-Coated Glass as the Substrate Material. *Anal. Chem.* **2017**, *89*, 8129–8133.
24. Wu, F.; Zhou, B.; Wang, J.; Zhong, M.; Das, A.; Watkinson, M.; Hing, K.; Zhang, D.W.; Krause, S. Photoelectrochemical Imaging System for the Mapping of Cell Surface Charges. *Anal. Chem.* **2019**, *91*, 5896–5903.
25. Tu, Y.; Ahmad, N.; Briscoe, J.; Zhang, D.W.; Krause, S. Light-Addressable Potentiometric Sensors Using ZnO Nanorods as the Sensor Substrate for Bioanalytical Applications. *Anal. Chem.* **2018**, *90*, 8708–8715.
26. Nakamura, S.; Senoh, M.; Mukai, T. P-GaN/N-InGaN/N-GaN Double-Heterostructure Blue-Light-Emitting Diodes. *Jpn. J. Appl. Phys.* **1993**, *32*, L8–L11.
27. Lin, H.W.; Lu, Y.J.; Chen, H.Y.; Lee, H.M.; Gwo, S. InGaN/GaN nanorod array white light-emitting

diode. *Appl. Phys. Lett.* **2010**, *97*, 98–101.
28. Matioli, E.; Neufeld, C.; Iza, M.; Cruz, S.C.; Al-Heji, A.A.; Chen, X.; Farrell, R.M.; Keller, S.; DenBaars, S.; Mishra, U.; et al. High internal and external quantum efficiency InGaN/GaN solar cells. *Appl. Phys. Lett.* **2011**, *98*, 2009–2012.
29. Kibria, M.G.; Chowdhury, F.A.; Zhao, S.; AlOtaibi, B.; Trudeau, M.L.; Guo, H.; Mi, Z. Visible light-driven efficient overall water splitting using p-type metal-nitride nanowire arrays. *Nat. Commun.* **2015**, *6*, 1–8.
30. Wallys, J.; Teubert, J.; Furtmayr, F.; Hofmann, D.M.; Eickhoff, M. Bias-enhanced optical ph response of group III-nitride nanowires. *Nano Lett.* **2012**, *12*, 6180–6186.
31. Maier, K.; Helwig, A.; Müller, G.; Becker, P.; Hille, P.; Schörmann, J.; Teubert, J.; Eickhoff, M. Detection of oxidising gases using an optochemical sensor system based on GaN/InGaN nanowires. *Sensors Actuators, B Chem.* **2014**, *197*, 87–94.
32. Riedel, M.; Hölzel, S.; Hille, P.; Schörmann, J.; Eickhoff, M.; Lisdat, F. InGaN/GaN nanowires as a new platform for photoelectrochemical sensors – detection of NADH. *Biosens. Bioelectron.* **2017**, *94*, 298–304.
33. Taylor, E.; Fang, F.; Oehler, F.; Edwards, P.R.; Kappers, M.J.; Lorenz, K.; Alves, E.; McAleese, C.; Humphreys, C.J.; Martin, R.W. Composition and luminescence studies of InGaN epilayers grown at different hydrogen flow rates. *Semicond. Sci. Technol.* **2013**, *28*.
34. Martin, R.W.; Edwards, P.R.; O'Donnell, K.P.; Mackay, E.G.; Watson, I.M. Microcomposition and Luminescence of InGaN Emitters. *Phys. status solidi* **2002**, *192*, 117–123.
35. Tauc, J.; Grigorovici, R.; Vancu, A. Optical Properties and Electronic Structure of Amorphous Germanium. *Phys. status solidi* **1966**, *15*, 627–637.
36. Viezbicke, B.D.; Patel, S.; Davis, B.E.; Birnie III, D.P. Evaluation of the Tauc method for optical absorption edge determination: ZnO thin films as a model system. *Phys. status solidi* **2015**, *252*, 1700–1710.
37. Brown, G.F.; Iii, J.W.A.; Walukiewicz, W.; Wu, J. Solar Energy Materials & Solar Cells Finite element simulations of compositionally graded InGaN solar cells. *Sol. Energy Mater. Sol. Cells* **2010**, *94*, 478–483.
38. Can, M.; Havare, A.K.; Aydın, H.; Yagmurcukardes, N.; Demic, S.; Icli, S.; Okur, S. Electrical properties of SAM-modified ITO surface using aromatic small molecules with double bond carboxylic acid groups for OLED applications. *Appl. Surf. Sci.* **2014**, *314*, 1082–1086.
39. Hammer, M.S.; Deibel, C.; Pflaum, J.; Dyakonov, V. Effect of doping of zinc oxide on the hole mobility of poly (3-hexylthiophene) in hybrid transistors. *Org. Electron.* **2010**, *11*, 1569–1577.
40. Ebaid, M.; Kang, J.H.; Lim, S.H.; Ha, J.S.; Lee, J.K.; Cho, Y.H.; Ryu, S.W. Enhanced solar hydrogen generation of high density, high aspect ratio, coaxial InGaN/GaN multi-quantum well nanowires. *Nano Energy* **2015**, *12*, 215–223.
41. Kobayashi, N.; Morita, R.; Narumi, T.; Yamamoto, J.; Ban, Y.; Wakao, K. Flat-band potentials of GaN and InGaN/GaN QWs by bias-dependent photoluminescence in electrolyte solution. *J. Cryst. Growth* **2007**, *298*, 515–517.
42. Miyamoto, K.; Sugawara, Y.; Kanoh, S.; Yoshinobu, T.; Wagner, T.; Schöning, M.J. Image correction method for the chemical imaging sensor. *Sensors Actuators B Chem.* **2010**, *144*, 344–348.
43. George, M.; Parak, W.J.; Gerhardt, I.; Moritz, W.; Kaesen, F.; Geiger, H.; Eisele, I.; Gaub, H.E. Investigation of the spatial resolution of the light-addressable potentiometric sensor. *Sensors Actuators, A Phys.* **2000**, *86*, 187–196.
44. Kumakura, K.; Makimoto, T.; Kobayashi, N.; Hashizume, T.; Fukui, T.; Hasegawa, H. Minority carrier diffusion lengths in MOVPE-grown n- and p-InGaN and performance of AlGaN/InGaN/GaN double heterojunction bipolar transistors. *J. Cryst. Growth* **2007**, *298*, 787–790.